Table 2: H/V Coupling Before and After Correction of Central Orbit

seed	submatrix determinants before correction			
1	DET A= 1.000	DET B= .000	DET C= .000	DET D= 1.000
2	DET A= 1.006	DET B= -.006	DET C= -.006	DET D= 1.006
3	DET A= 1.003	DET B= -.003	DET C= -.003	DET D= 1.003
4	DET A= 1.002	DET B= -.002	DET C= -.002	DET D= 1.002
5	DET A= 1.015	DET B= -.015	DET C= -.015	DET D= 1.015
6	DET A= 1.010	DET B= -.010	DET C= -.010	DET D= 1.010
7	DET A= 1.000	DET B= .000	DET C= .000	DET D= 1.000
8	DET A= 1.004	DET B= -.004	DET C= -.004	DET D= 1.004
9	DET A= 1.003	DET B= -.003	DET C= -.003	DET D= 1.003
10	DET A= 1.002	DET B= -.002	DET C= -.002	DET D= 1.002

seed	submatrix determinants after correction			
1	DET A= 1.000	DET B= .000	DET C= .000	DET D= 1.000
2	DET A= 1.000	DET B= .000	DET C= .000	DET D= 1.000
3	DET A= 1.000	DET B= .000	DET C= .000	DET D= 1.000
4	DET A= 1.000	DET B= .000	DET C= .000	DET D= 1.000
5	DET A= 1.000	DET B= .000	DET C= .000	DET D= 1.000
6	DET A= 1.000	DET B= .000	DET C= .000	DET D= 1.000
7	DET A= 1.000	DET B= .000	DET C= .000	DET D= 1.000
8	DET A= 1.000	DET B= .000	DET C= .000	DET D= 1.000
9	DET A= 1.000	DET B= .000	DET C= .000	DET D= 1.000
10	DET A= 1.000	DET B= .000	DET C= .000	DET D= 1.000

Conclusions and Comments

The results detailed above indicate that machine performance is acceptable for errors consistent with the error budget. Ongoing work will include more accurate modeling of dipole roll and errors in π-bend alignment and excitation. It will determine individual error sensitivities by looking at beam performance response to variations in individual error levels, as well as the global response to multiple errors. Future work will establish the effect of magnetic field inhomogeneities in wiggler and beamline elements, and include H/V coupling in RF cavities

References

[1] D. Douglas, “Engineering Design Specifications for IR FEL Driver Transport System”, CEBAF-TN-96-026, 6 June 1996; D. Douglas, “Error Estimates for the IR FEL Transport System”, CEBAF-TN-96-035, 15 July 1996.

[2] *ibid*.

[3] D. Douglas, “IR FEL Driver Accelerator Design” CEBAF-TN-96-050, 27 September 1996.

[4] D. Douglas, “Engineering Design Specifications for IR FEL Driver Transport System”, CEBAF-TN-96-026, 6 June 1996

[5] D. Douglas, CEBAF Technical Note in preparation.

Geometric Aberrations

Figure 5 displays the phase space distortion parameters $\Delta\varepsilon_x/\varepsilon_x$ and $\Delta\varepsilon_y/\varepsilon_y$ *vs.* momentum for each of 10 random seeds, before and after correction of the on-momentum central orbit. A beam with 10 times the design geometric emittance of 0.16 mm-mrad (corresponding to a 13 mm-mrad normalized emittance at 42 MeV) was used in the DIMAD "`line geometric aberrations`" operation to evaluate the phase space distortion. Performance is acceptable in all cases, and approaches the ideal machine behavior after correction.

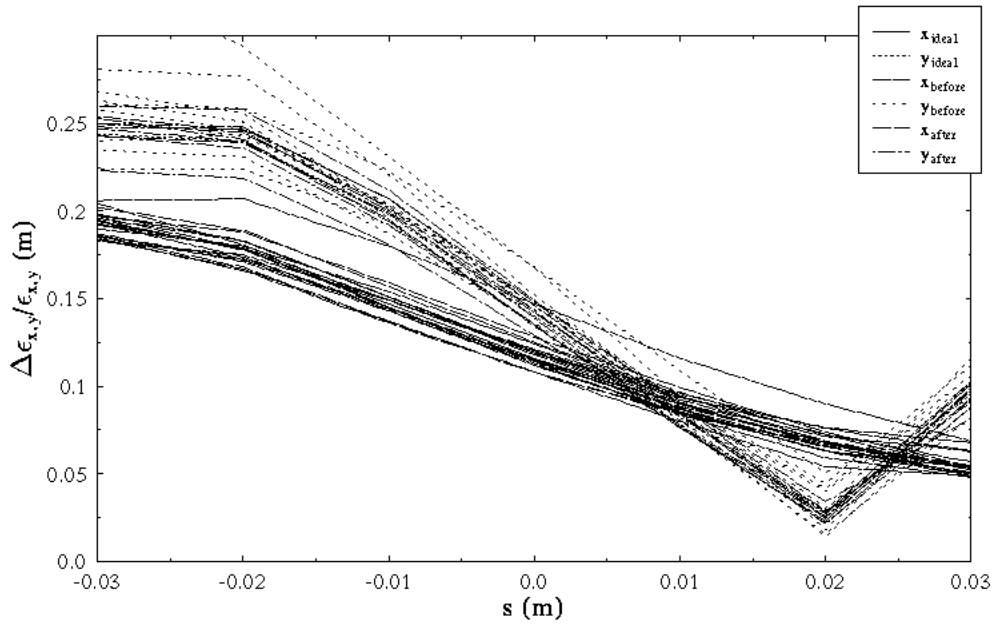

Figure 5: Phase space distortion of a beam with 10 times the design emittance as a function of momentum for 10 random seeds before and after correction of the on-momentum central orbit.

H/V coupling

Horizontal/vertical coupling about a specified orbit can be computed using the DIMAD "`rmatrix`" operation, which evaluates the linear transfer matrix about the orbit of interest and evaluates the determinants of the various transverse sub-blocks. Table 2 presents the results of this process for each random distribution studied, before and after correction of the central orbit. Before correction, the H/V coupling parameters `DET B` and `DET C` are small; after correction they are vanishingly small. The transport system is therefore not expected to experience inherent coupling problems. Any such difficulties will be due to magnetic field errors and/or coupling in the RF cavities, both of which will be evaluated in future simulations.

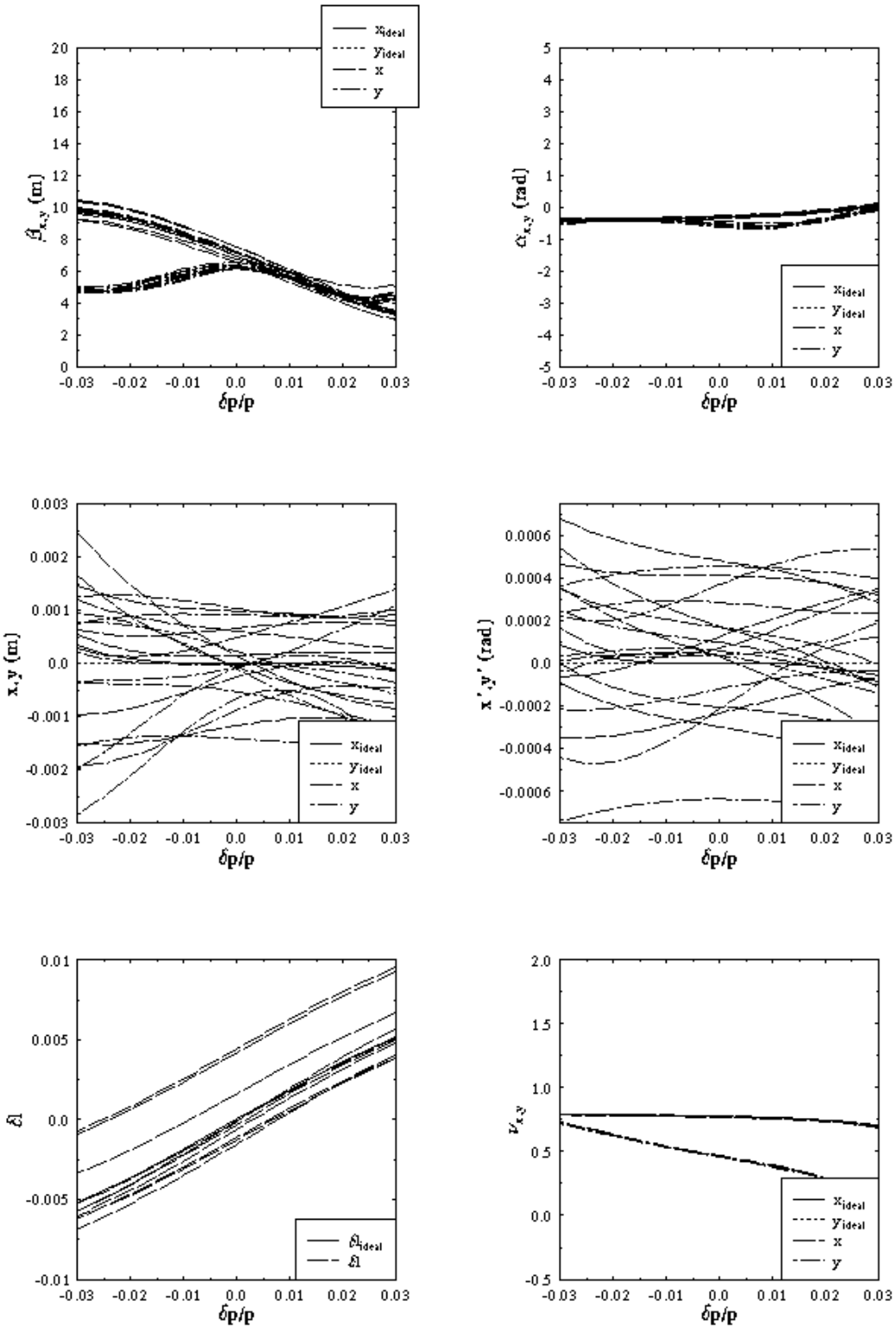

Figure 4b: Results of momentum scan of parameters at reinjection point after correction of on-momentum central orbit

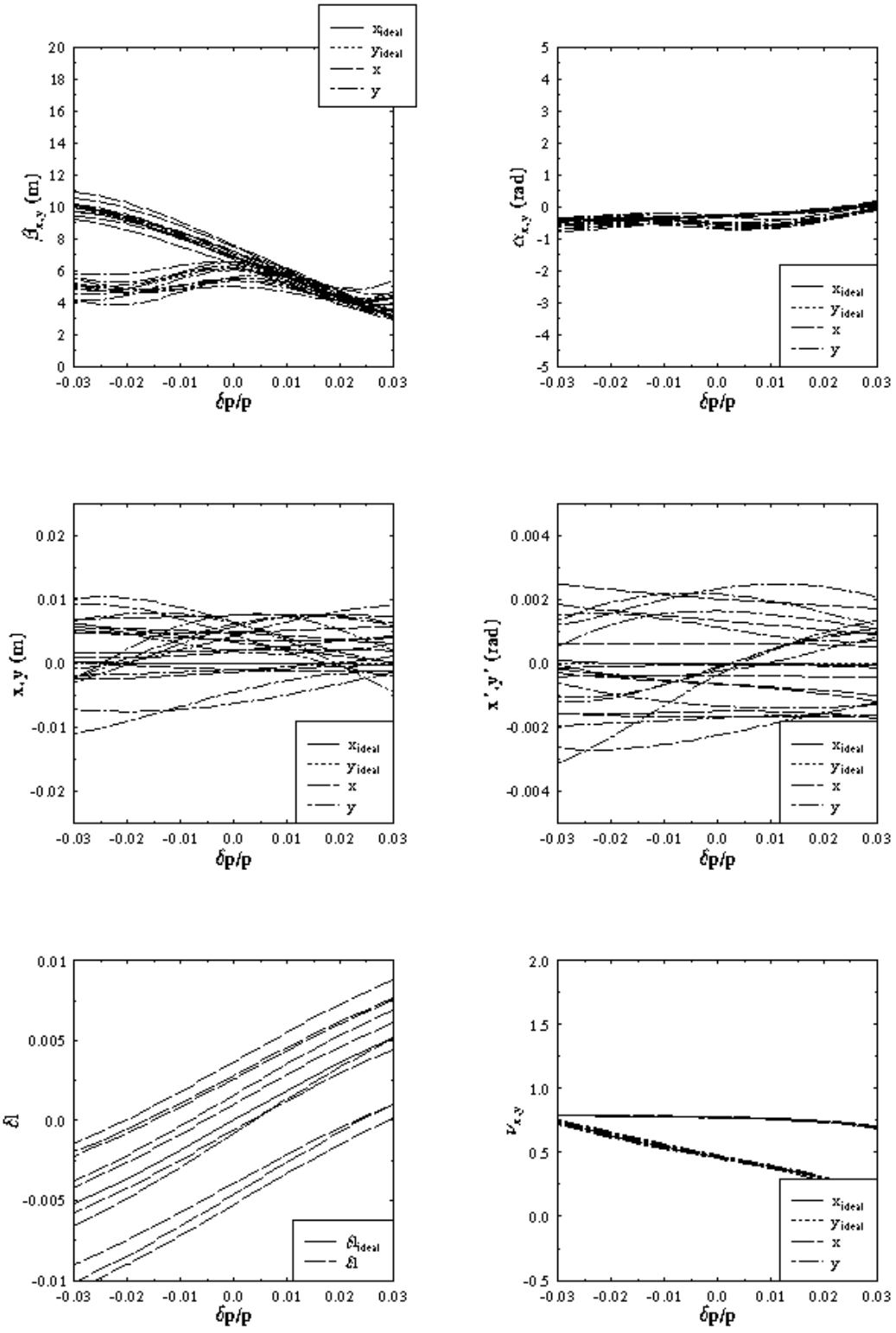

Figure 4a: Results of momentum scan of parameters at reinjection point before correction of on-momentum central orbit

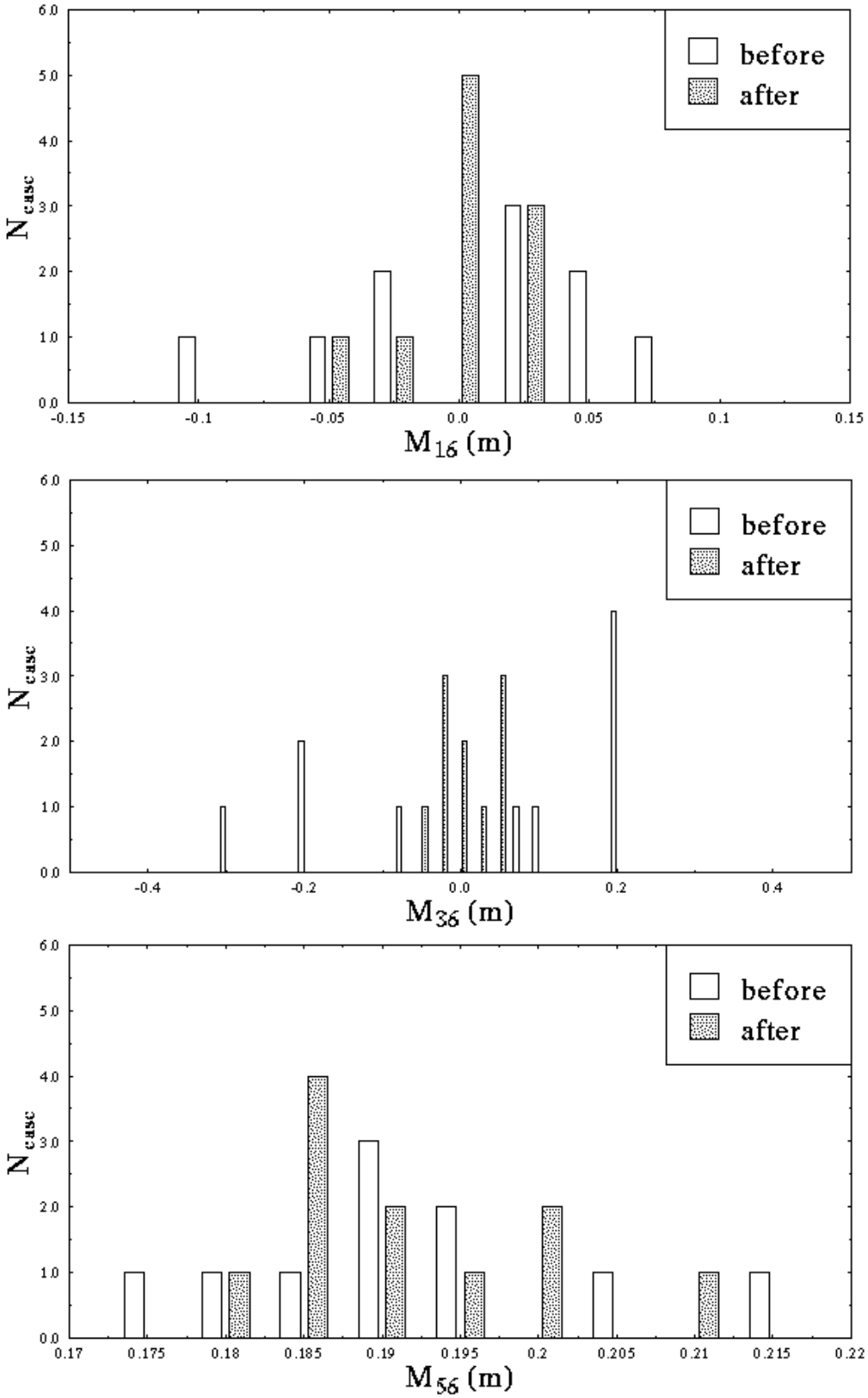

Figure 3: Distribution of M_{16}, M_{36}, and M_{56} before and after central orbit correction.

seed-dependent scatter in path length is well within the range of compensation available in the machine; the momentum dependence is nearly ideal. Beam envelope functions exhibit little dependence on orbit errors both on and off momentum, even before correction. They are nearly ideal after correction.

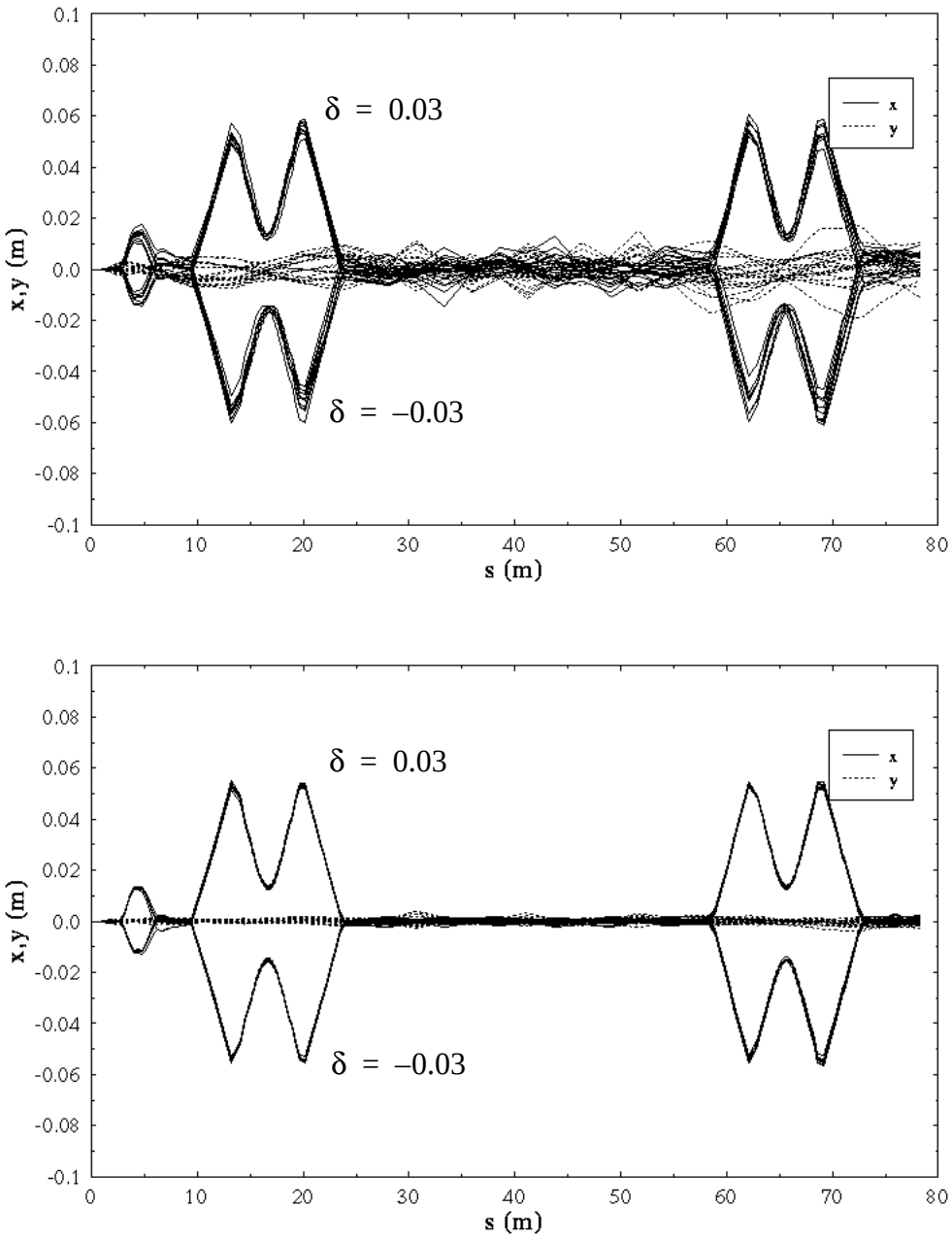

Figure 2: Off momentum orbits (at ±0.03 %) before (top) and after (bottom) correction of the on-momentum orbit.

Uncorrected orbits are typically at the several millimeter level, with peaks in excess of 1 cm; corrected orbits are typically at the few millimeter level, with peaks below 5 mm. Locations and causes of peaks in the remnant orbit are under investigation. One example of such a "problem" location is at a longitudinal displacement of ~6-7 m, where persistent horizontal peaks are seen in the remnant orbit. These occur at the high β_x point of the second triplet in the downstream matching telescope, and are driven by the fact that the position monitors in this region are all at points of smaller β_x (but larger β_y). Misalignments of the upstream and downstream monitors are then magnified by the relative betatron amplitude when the orbit is corrected. Such errors can be avoided by introduction of a single additional horizontal position monitor at the high β_x point, or at less cost by centering horizontally in the quadrupole during machine setup. The latter solution will probably be adopted, as it not only avoids peaks in the remnant orbit, but by construction generates a well steered injection orbit for transport through the first end loop.

Chromatic Behavior

Off-Momentum Orbits/Dispersions/Momentum Compaction. Figure 2 shows plots of off-momentum orbits (at ±0.03%) for ten random error sets before and after orbit correction. In this case, the correction is done *for the on momentum central orbit only*. We find that simple correction of just the on-momentum central orbit leads to generally adequate machine performance; the off-momentum orbits track the corresponding on-momentum orbits, indicating the correction is more or less local. If ongoing studies indicate the need to do so, the off-momentum orbits can be separately constrained during the orbit correction process as well, and/or dispersion correction can be activated during or after orbit correction.

Figure 3 provides histograms of dispersions and momentum compaction (specifically, M_{16}, M_{36}, and M_{56} from wiggler center to reinjection point) for each of the ten random seeds studied, before and after correction of the on-momentum central orbit. Before correction, horizontal dispersion and momentum compaction are fairly near design values, but spurious vertical dispersion can become rather large. This is probably due to the fact that Bates-type lattices tend to have large T_{346} values. Vertical quadrupole misalignments will cause angular kicks that couple to these aberrations and can thereby generate large effective vertical dispersion. Localized correction of the on-momentum orbit will compensate such effects at their source; this is seen in Figure 3, where we note that M_{16}, M_{36}, and M_{56} all return to near-design values following correction.

Momentum Scans of Orbit and Betatron Properties. Figure 4a and 4b present the results of momentum scans of beam position, angle, and lattice functions at the reinjection point, and path length variation and phase advance from wiggler to reinjection point, before and after correction of the on-momentum central orbit. The orbit correction process significantly reduces the final position and angular offsets and their variations with momentum. This is consistent with the above discussion. The

- *large amplitude behavior* - geometric aberrations and phase space distortion
- *H/V coupling*

Results for each category with errors, before and after correction, follow.

Central Orbit

Figure 1 displays horizontal and vertical central orbits for 10 random error sets before and after correction. All orbits remain within the 2 inch vacuum chamber before correction. All orbits are significantly improved by the correction process.

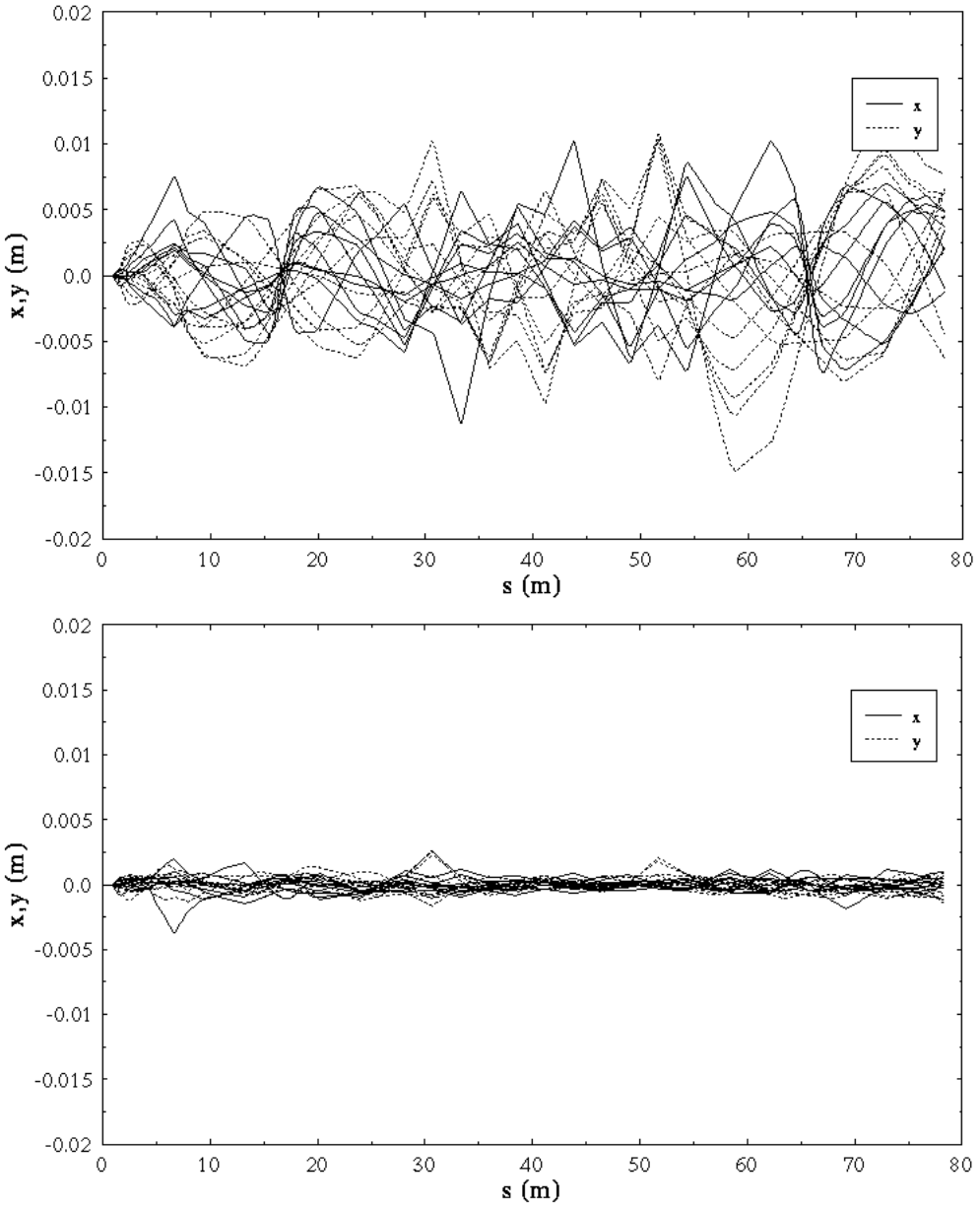

Figure 1: Central orbits for 10 seeds, before (top) and after (bottom) correction.

Following the above analysis, orbit correction was modeled using the DIMAD "`alignment fitting`" operation. The diagnostic and correction package is specified elsewhere [4] and will be discussed in detail in a forthcoming CEBAF Technical Note [5]. We make the specific comment that the simulation assumes that positional information is provided by both BPMs *and* beam viewers as specified in Reference [4]. The BPM distribution in [4] is probably not, in and of itself, sufficiently dense to correct the orbit using an automated process, particularly in the backleg. The process simulated here more closely resembles the action of a trained operator using BPMs and viewers (and possibly quad centering) to locate and correct the misaligned orbit.

Automated orbit correction will require implementation of a "complete" set of BPMs, providing precision positional information (in at least the focussing plane) at each quadrupole in the backleg and in both planes at various points through the end loops. The availability of such diagnostics is at present under evaluation from cost and engineering perspectives.

After correction, the above performance analysis was repeated to quantify machine behavior in a "nominal" operating mode. Results before and after correction are discussed below.

Two additional comments are in order. First, because of the aforementioned restriction on block misalignments, errors were not imposed on the π-bends. This is not a major deficiency in the model, because at present we are using ideal magnet models, so that the π-bend is (linearly) a -I transform horizontally and a drift vertically. Provided the alignment is at the millimeter level, the ideal π-bend will have little effect. Similarly, π-bend powering errors were not included inasmuch as these magnets are independently shunted and will be individually excited based on magnetic measurements and beam behavior. When magnetic inhomogeneities are included, the influence of such misalignments and mispowerings are more significant. They will be included in future simulations through use of correlated leading/trailing kicks.

Secondly, as DIMAD (and any other matrix code) expands the motion about a reference orbit, it will not properly model the effect of a dipole roll. The necessary information is not included in the matrix, which describes differential motion about (a potentially rolled) circular arc. H/V coupling through skewed dipole focussing is properly modeled, but the out-of-midplane projection of the orbit is missed. A reasonable linearly perturbative description of roll effects can be made by introducing out of midplane kicks adjacent to the dipoles; this will be done in future simulations.

Results

General criteria for machine/beam performance are as follows:

- *central orbit behavior*
- *chromatic behavior* - of the orbit (off momentum orbits, dispersion, and momentum compaction), and of beam properties about the orbit (beam envelopes, phase)

beamlines subtending angles of order 1/2 radian will experience some tens of percent error in the details of the misaligned position of the element relative to the reference orbit. As we are interested in only order-of-magnitude effects of misalignments this was deemed unimportant. Alignment errors were therefore imposed using this mechanism with the DIMAD maximum allowed cutoff of 2 σ to evaluate ten random error sets using RMS error values as given in Table 1.

Starting seeds for the ten random number distributions were the sequence 111111111, 222222221, 333333333, 444444443, 555555555, 666666665, 777777777, 888888887, 999999999, and 101010101. The tuning studied was the "19 centimeter momentum compaction" version of the 6 September 1996 optics solution [3].

Table 1: RMS Error Values Used in Simulations

Element Type	σ_x^{in} (mm)	σ_x^{out} (mm)	σ_y^{in} (mm)	σ_y^{out} (mm)	σ_z (mm)	$\sigma_{z'}$ (mrad)	$\sigma_{\delta p/p}$ (mrad)
quadrupoles main trim	 0.5 0.5	 0.5 0.5	 0.5 0.5	 0.5 0.5	 5 5	 1 1	 1 2.5
BPMs	0.5	-	0.5	-	5	0	-
sextupoles	1	1	1	1	1	1	2.5
extraction chicane dipoles	1	1	1	1	1	1	1
optical cavity chicane dipoles	1	1	1	1	1	1	1
reverse bends	1	1	1	1	1	1	1

The orbit was modeled and beam performance studied using the following standard DIMAD operations:

- "`reference orbit display`" - to display the misaligned orbit,
- "`rmatrix`" - to determine the linear transfer matrix and H/V coupling around the misaligned orbit,
- "`detailed chromatic analysis`" - to perform a momentum scan around the misaligned orbit, and
- "`line geometric aberrations`" - to examine large amplitude behavior and quantify phase space distortion due to geometric aberrations.

Simulation of Alignment and Powering Errors in the IR FEL Driver Beam Transport System

D. Douglas

Abstract

Results of performance simulations for the IR FEL driver transport system in the presence of alignment and excitation errors are presented. Acceptable machine behavior is expected for errors consistent with a previously specified error budget [1].

Machine Model

The purpose of this study was to certify those portions of an analytically derived project error budget [2] relating to DC (time constant) errors. A model of the IR FEL beam transport system was constructed using DIMAD. Magnet alignment and DC excitation errors consistent with the project error budget were imposed on beamline elements, and various machine performance criteria were examined for each of several randomly selected suites of errors. Results for the machine performance criteria were then evaluated to verify that machine parameters were adequately well behaved in the presence of errors.

The beamline model studied comprised a DIMAD implementation of the wiggler to reinjection point transport. This is the longest and largest acceptance optics module in the machine, and contains the majority of the transport elements. All magnets were modeled as ideal; the standard TRANSPORT end field model with a K_1 of 0.45 was employed for the dipoles. The wiggler (from center to end) was modeled as parallel faced dipole blocks. Alignment and excitation errors were imposed on "small" elements - quadrupoles, extraction chicane and optical cavity chicane dipoles, sextupoles, and beam position monitors - using the DIMAD "`misalignment data definition`" and "`set misalignments`" operations. Alignment option 2 (misalignments imposed along the chord between entry and exit points) was used for magnets, and alignment option 1 (misalignments about the entrance point) was used for BPMs (which were modeled with zero length); a gaussian distribution with the DIMAD maximum allowed error cutoffs of 6 σ was employed to generate ten random error sets with RMS error values as given in Table 1.

Alignment and excitation errors were imposed on the reverse bends (which have been subdivided to increase the accuracy of chromatic analysis operations and to prepare for error multipole studies) using the DIMAD "`block misalignment`" operation. This operation nominally is applied to only straight beam lines or beamlines subtending angles of 0.1 radian or less. The reverse bends subtend ~0.5 radian, so the source code for the operation was examined to understand any possible pitfalls. It was found that "`block misalignment`" employs small angle approximations to establish the location of the beamline block entry/exit points, so that